Flow Measurement and Instrumentation 95 (2024) 102502

Contents lists available at ScienceDirect

Flow Measurement and Instrumentation

journal homepage: www.elsevier.com/locate/flowmeasinst

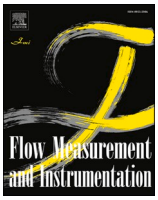

On the effect of aeration on laser ranging measurements of free water surface

Benjamin Bizjan [a], Marko Hočevar [a], Sabina Kolbl Repinc [b], Gašper Rak [b,*]

[a] University of Ljubljana, Faculty of Mechanical Engineering, Aškerčeva 6, 1000 Ljubljana, Slovenia
[b] University of Ljubljana, Faculty of Civil and Geodetic Engineering, Jamova 2, 1000 Ljubljana, Slovenia

ARTICLE INFO

Keywords:
Aerated flow
Free surface
Laser scanning
LIDAR
Non-stationary surface

ABSTRACT

Aerated flows pose both challenges and opportunities in the measurement of free water surface. In this study, an amplitude-modulated continuous wave scanning LIDAR device was used to measure a distance from the device sensor to the water column surface subjected to different degrees of aeration, while reference measurements were performed by high-speed imaging. Different aeration conditions were generated by variation of the air flow rate supplied to the liquid and by using perforated plates with different hole arrangements. The LIDAR device was shown to produce level readings consistently below visible water levels. The measurement error of the LIDAR method is largely determined by the volume fraction of air in water and was lowest at about 0.1 air volume fraction. The error increases linearly until a very high air volume fraction (i.e., above 0.55), while the LIDAR method also performs poorly in unaerated water. Although the measurement uncertainty of LIDAR in the range of aerated water is by at least an order of magnitude higher than in the case of measuring dry solid surfaces, the method is viable for free surface measurement under low to moderate aeration conditions that don't produce excessive foaming.

1. Introduction and background

Aerated free-surface flows commonly occur in both natural and man-made hydraulic structures, particularly in spillways [1,2], channel confluences [3], fish passages [4] and flows across rough channel beds [5]. Flows encountered in such hydraulic structures undergo varying degrees of air entrainment (also known as self-aeration), the mechanism of which has been investigated extensively [6–8]. The field of experimental hydraulic measurements, instrumentation and data processing has seen many decades of research, with review available in several monographs [9–11]. Nevertheless, in measurement of the liquid's free surface topography, the presence of complex turbulent multiphase flow structures such as entrained air bubbles dictate a different selection of measurement methods than in unaerated, low fluctuation flows [12]. There are numerous different methods for measuring the free water surface, a recent review provided by Rak et al. [13]. Point measurements methods can be conducted by instruments such as U-manometers [14], point gauges [5], wave probes [15] or ultrasonic devices [16]. Although accurate, these methods can be time-consuming if an extensive or complex free water surface topography is to be measured, don't allow for measuring unsteady flows, are intrusive (except for ultrasonic distance meters) and often perform poorly with turbulent and aerated flows [17]. To address these issues, non-contact (remote sensing) optical methods based on laser ranging [3,18,19], laser triangulation [20], or camera imaging through sidewalls [21,22] and by 3D-stereoscopic algorithms [23] were investigated recently. Rapid advances in both measurement hardware and data processing algorithms have made these non-contact methods a viable alternative to more time-consuming and mostly intrusive conventional methods.

Laser ranging is one of the more widely used remote sensing free surface measurement methods and is better known under the name of light detection and ranging (LIDAR). The robustness and versatile use of the LIDAR method is reflected in a number of different fields of application in terrestrial scanning [18,24,25] as well as free surface flow measurement including hydraulic jumps [19,26,27], undular tidal bores [28] and confluence flows [3]. LIDAR technology operates by emitting a laser beam towards the surface of interest where it is partly reflected to the receiver, and the most established method for calculation of the distance to the surface is by time-of-flight (ToF) measured from phase shift of the amplitude-modulated laser [17], although

* Corresponding author.
E-mail addresses: benjamin.bizjan@fs.uni.lj.si (B. Bizjan), marko.hocevar@fs.uni.lj.si (M. Hočevar), sabina.kolbl-repinc@fgg.uni-lj.si (S. Kolbl Repinc), gasper.rak@fgg.uni-lj.si (G. Rak).

https://doi.org/10.1016/j.flowmeasinst.2023.102502
Received 20 July 2023; Received in revised form 11 November 2023; Accepted 21 November 2023
Available online 26 November 2023

frequency-modulation-based techniques have also seen significant developments and prominence recently [29]. When ranging free water surface, laser light reflection can be either of specular type (reflection angle equals beam incident angle) or diffuse type where reflection occurs in a broad spectrum of angles [17]. Several studies [17,19,30] have so far determined LIDAR to be best suited for fully aerated flows while performing poorly in unaerated or partly aerated flows. In the absence of entrained air, droplets, and other features that enhance the free surface roughness of water, laser light reflections are predominantly of the specular type and can only be detected by the device receiver for a very narrow range of reflection angles [18]. On the other hand, when water is sufficiently aerated, diffuse reflection is more likely as the emitted laser beam is diffusely reflected off the bubbles on the water surface as well as those submerged below the surface [17].

Having said that, mechanisms of flow aeration are highly complex and vary depending on the type of hydraulic structure and the inflow conditions [31,32]. Apart from entrained bubbles, droplets emerging from the free water surface can also have a substantial effect on the performance of ranging measurements [33]. Rak et al. [17] utilized a glass tank with a calm water surface to study the effect of flow aeration and foaming on the accuracy of the LIDAR measurement method. Results showed a reduction in the water level measurement error for aerated flow with soap foam as opposed to unaerated flow and foam-free aerated flow, while the water depth had little effect on the measurement error.

While several studies so far have demonstrated a positive effect of flow aeration on LIDAR measurement accuracy and reliability, this paper aims to investigate the effects of aeration parameters on the performance of LIDAR free water surface ranging on a quantitative level. These parameters will include bubble size and concentration, as well as varying degrees of free water surface level fluctuations due to the surfacing of bubbles. Results of the present study are expected to improve the understanding of flow aeration on laser ranging measurement uncertainty, and the method's applicability to hydraulic engineering measurements under different flow conditions.

2. Materials and methods

The principal challenge in investigating the flow aeration effects on LIDAR performance is building an experimental rig enabling controlled and repeatable generation of immersed air bubbles. One of the possible approaches was proposed by Chanson et al. [34] who employed a plunging water jet and an induction trumpet to draw the air into the wave flume filled with liquid (freshwater and seawater were used) through a narrow gap. In this study, the volume fraction of entrained air was measured by a phase-detection probe and signal processing thereof utilizing a bubble counting algorithm. In the present study, we propose a different aeration mechanism based on the injection of air bubbles and high-speed imaging as the reference method for measuring the free surface level and air volume fraction. The aerated flow was generated in a vertical cylinder-shaped column opened at the top (Fig. 1). The column (plexiglass tube of 0.5 m length and 94 mm internal diameter) was divided into two sections separated by a replaceable plastic perforated plate with a matte surface. Pressurized air was fed into the lower section at a flow rate measured via a rotameter and controlled by adjusting the air pressure that was measured immediately below the column. The column section above the perforated plate was filled with water, resulting in the formation of bubbles above the plate that moved upwards towards the water surface. Three different plates with circular perforations (perforation diameter d of 0.2, 0.32, and 0.5 mm) were used at flow rates Q between 0 and 70 L/min. Perforation spacing δ (equal in both horizontal directions, Fig. 1) was 11 mm for plates with 0.2 mm and 0.32 mm holes (resulting in porosity of 0.027 % and 0.069 %, respectively), while 0.5 mm holes were spaced 16 mm apart (resulting porosity of 0.096 %). In this manner, multiphase flows with varying air volume fractions and mean bubble sizes were generated (Fig. 1).

The water surface level of the aerated flow in the column was measured by a SICK LMS4121R-13000 two-dimensional laser scanner based on LIDAR technology (SICK AG. "[35]. The device operates on an amplitude-based continuous wave (AMCW) phase correlation technique to determine ToF and resulting ranging distance. The laser beam (visible red, 650 nm wavelength, 1 mm diameter) was manipulated by a rotating prism, achieving a scanning angle of 70°, an angular resolution of 1/12° (a total of 841 measurement points per scan) and a scanning rate of 600

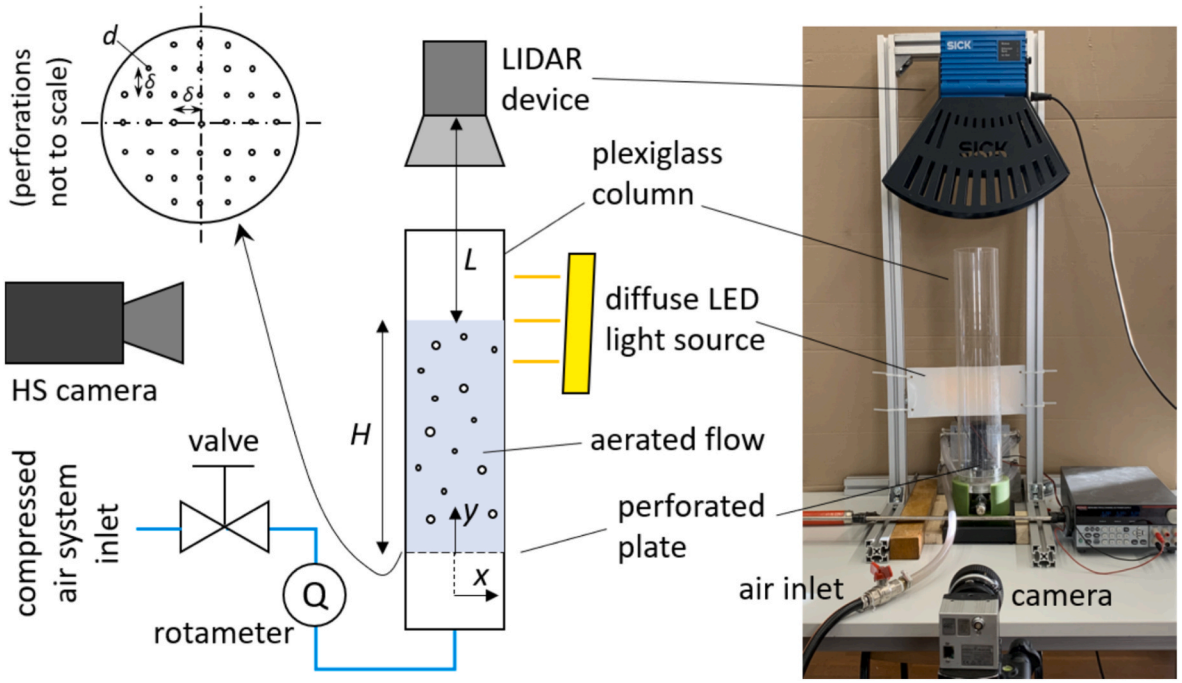

Fig. 1. Experimental set-up for laser ranging of the surface of aerated water column.

profiles per second. The scanner's recommended operating range was between 0.7 m and 3 m from the device emitter/receiver to the object of interest, while its systematic error quoted by the manufacturing was expected to be within ±1 mm for ranging measurement of solid surfaces.

Prior to the start of aeration, the column was filled with $H_0 = 110$ mm of water (measured from the perforated plate to the water level). The LIDAR device was installed above the column 800 mm from the perforated plate measured from the midpoint position of the laser scanning angle where the laser beam pointed vertically into the center of the plate. Such an arrangement was selected to ensure that measured distances fell close to the recommended minimum measurement distance, thus minimizing the measurement uncertainty and maximizing available angular scanning resolution across the liquid column. Since the scanning angle of the LIDAR device (70°) was much larger than the actual angle where aerated liquid was present (about 8°), the ranging data outside of this region was discarded.

To assess the measurement performance of the LIDAR device, reference water level measurements were conducted by a high-speed camera (Fastec HiSpec 4 Mono, 1696 × 1080 pixels region of interest, 600 frames/s, 0.085 mm pixel size, 40 μs shutter time, Nikkor 50 mm f/1.2 lens with f/4 aperture) recording in the focal plane identic to the laser scanning plane. The camera's focal plane was illuminated by diffuse LED lighting mounted on the opposite side of the liquid column so that light was transmitted through the liquid. Due to the large rejection rate of LIDAR data (about 80 %), the comparison of instantaneous free surface profiles to imaging measurements was not feasible, and a time-averaging statistical approach was employed instead across a data acquisition period of 2.0 s for both methods (data acquisition for both methods was synchronized to the same time interval).

In our experiments, the water depth H (Fig. 1) was measured indirectly by measuring the distance L between the LIDAR receiver and the water surface and subtracting it from dry column distance (deeper water results in lower distance L). The measurement uncertainty of measuring H can vary significantly depending on the measurement setup (namely, depth H, distance L, and LIDAR specifications). In a measurement arrangement shown in Fig. 1, L is much larger than H, thus the relative measurement uncertainty of depth measurement is also higher compared to the measurement of L – by a factor of L/H. For the sake of the present-investigation result comparability to other studies, our analysis will focus on the measurement accuracy of LIDAR distance measurement near the lower end of the measurement distance range.

3. Results and discussion

3.1. Aeration phenomena and flow regimes

The effect of aeration on flow conditions inside the column is shown in Fig. 2 expressed in dimensional (aeration flow rate Q) and nondimensional terms as air volume fraction α:

$$\alpha = 1 - \frac{H_0}{L_P - L} \tag{1}$$

In Eq. (1), $H_0 = 110$ mm is the initial unaerated water depth, $L_P = 800$ mm is the distance from the perforated plate to the receiver and L is the distance to the free surface measured by LIDAR (i.e., ranging distance). Evidently, as the flow rate of injected air increased from 0 to 70 L/min ($\alpha = 0 \ldots 0.394$), the water surface was gradually elevated from 110 mm to 230 mm and became increasingly perturbed, with visible foaming and droplet ejection above the surface. Also, when the aeration flow rate exceeded 20 L/min ($\alpha = 0.228$), the aerated liquid became completely opaque.

A closer view of the free water surface region shown in Fig. 3 for different operating conditions reveals that aeration rates below 10 L/min ($\alpha = 0.141$) produce a stable water surface with little foaming and visible individual submerged bubbles as well as low amplitude waving. As Q is further increased, the surface is destabilized by the onset of large amplitude waves, and the upper boundary of foaming bubbles moves further away from the boundary of bulk liquid. Also, as demonstrated by Fig. 4, under low and medium aeration conditions (consider the example of $Q = 10$ L/min), the liquid surface waves visibly intermix with foamy structures containing mostly air. However, at higher aeration rates, (consider examples of $Q = 20$ L/min and 40 L/min), the oscillations of bulk liquid are no longer visible due to high bubble foam concentration rendering the liquid opaque. The mean bubble diameter near the free surface at 10 L/min can be visually estimated to 3.4 mm for 0.2 mm holes, 4.7 mm for 0.32 mm holes, and 5.3 mm for 0.5 mm holes and does

Fig. 2. Aeration flow rate effect on water in the column ($d = 0.5$ mm, $\delta = 16$ mm).

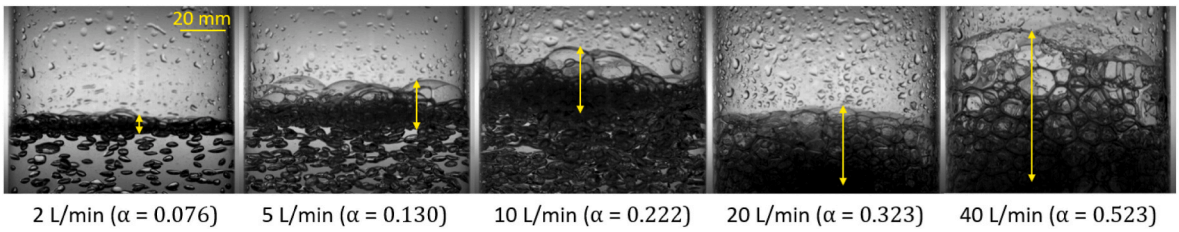

Fig. 3. The effect of aeration flow rate on water in the column ($d = 0.32$ mm, $\delta = 11$ mm). The region between the bulk liquid boundary and the upper boundary of foaming air bubbles is marked by a double-pointed arrow.

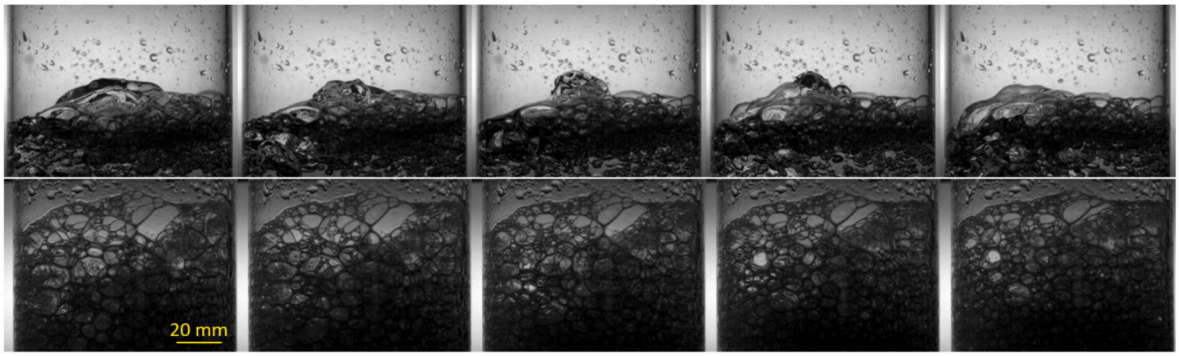

Fig. 4. Temporal development of flow structures for two aeration rates ($d = 0.32$ mm, $\delta = 11$ mm). Upper row: $Q = 10$ L/min ($\alpha = 0.222$), lower row: $Q = 40$ L/min ($\alpha = 0.523$), frame separation 25 ms.

not vary significantly in the 5 … 20 L/min range of Q. Due to the high bubble concentration, it was not possible to determine bubble diameters at higher aeration flow rates. For this reason, LIDAR performance will be assessed concerning the air volume fraction in the water that can be measured more reliably.

3.2. LIDAR and image processing result comparison

To obtain reference water levels, high-speed images were processed in MATLAB using the following methodology. First, the complete image sequence was loaded as a 3D matrix consisting of 1169 monochrome images represented by 8-bit matrices with 1696 × 1080 elements. Then, each image was cropped in the horizontal direction to the width of 1035 pixels (Fig. 5a, cropping area marked by dashed lines) so that the region of -44 mm $< x <$ 44 mm was retained (coordinate system shown in Fig. 5a). In the next step, median value (Fig. 5b) of the cropped 3D image matrix was calculated, followed by application of a 2D median filter (Fig. 5c) to remove droplets deposited on the column wall. The boundary line between darker aerated water and brighter background was then selected as our reference water surface and was acquired manually

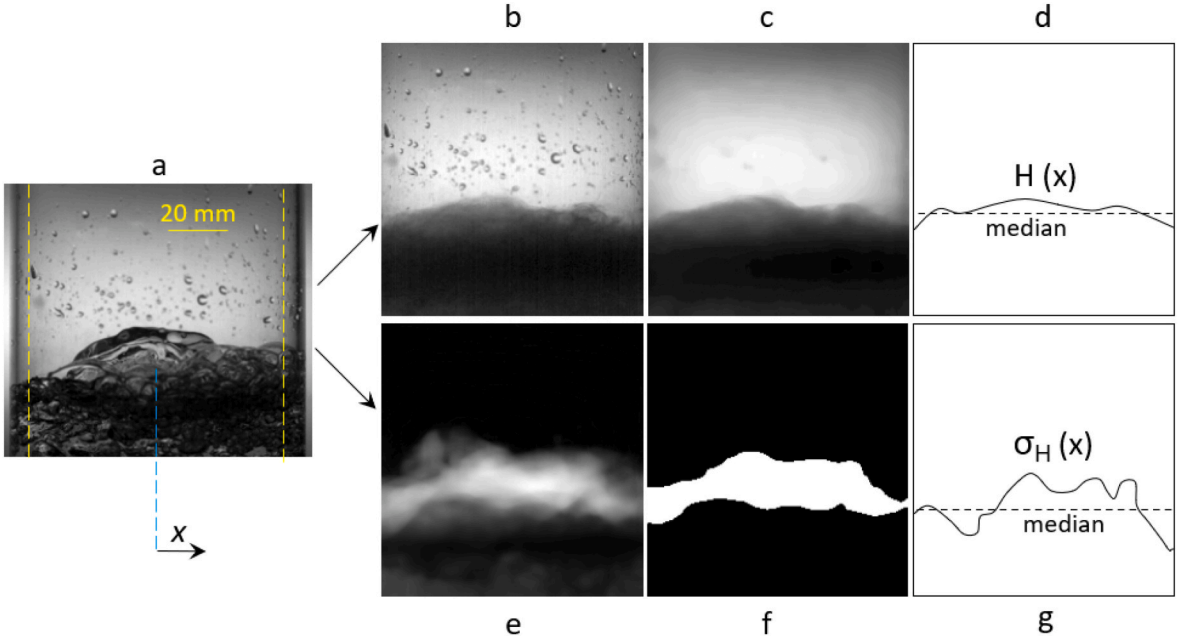

Fig. 5. Image processing methodology for water level measurements: input image (a), median image (b), median-filtered median image (c), median water level curve (d), normalized standard deviation image (e), binary image (f), median standard deviation of the water level curve (g).

in the *ImageJ* software. Finally, the acquired boundary points (20–30 for each median image) were subjected to a modified Akima interpolation algorithm to obtain smooth curves of water level H(x) sampled in the same discrete coordinates as LIDAR ranging data (Fig. 5d).

The behavior of the free water surface was further characterized by calculating the standard deviation of water level fluctuations. For this purpose, the cropped 3D image matrix (sample image shown in Fig. 5a) was used to calculate the standard deviation of the complete matrix. The resulting standard deviation field was normalized to its maximum value (Fig. 5e), and then to a binary image with a 0.45 Gy level threshold (Fig. 5f). In the final step, the water height standard deviation profile σ_H(x) was calculated as the sum of white pixels in every column of the binary image along the x-axis (Fig. 5g).

It is worth noting that although the presented high-speed image processing methodology was intended to produce reference measurements, significant measurement uncertainty is involved due to the complexity and opacity of highly aerated flows. Under some operating conditions, it is difficult to provide an unambiguous definition of the water surface location - whether it is the uppermost foaming region with very little water or an invisible aerated liquid layer below the apparent visible surface. Nevertheless, considering the careful manual segmentation of air and aerated water regions, the reference method is still significantly more accurate than LIDAR, where no verification of the beam reflection depth could be made, and reflections could occur at a wide variety of distances ranging from the foam above water level to the bulk liquid deep underneath. As will be discussed in the following section, LIDAR devices are prone to overestimation of distance to the free water surface.

Speaking of the LIDAR measurement and data processing methodology, the elevation profile of the free water surface in the column was scanned so that the angle of laser beam incidence was 0° in the center of the column, and the distance from the perforated plate to the receiver was L_P = 800 mm. LIDAR data was considered in the ±4° polar coordinate range from the column center that encompassed the water surface and corresponded to approximately ±44 … 48 mm in cartesian coordinates, depending on the distance of reflection points from the LIDAR receiver (only measurements with over 5 % remission were considered in analysis).

Although high-speed camera measurements covered the complete inner diameter of the column (±47 mm), the range for comparison was selected in the $-44\ \text{mm} < x < 44\ \text{mm}$ range where camera measurement coordinates overlapped with LIDAR coordinates under all operating conditions. The annular region corresponding to the outermost 3 mm of the liquid column radius was discarded to avoid erroneous measurements due to image distortion or laser beam reflections from the column wall.

A comparison of LIDAR- and camera-measured water level profiles ($H(x) = L_P\text{-}L(x)$) is shown in Fig. 6 for selected operating points. Presented $H(x)$ profiles suggest that the mean water level across the column width increases with Q, while the deviation between camera- and

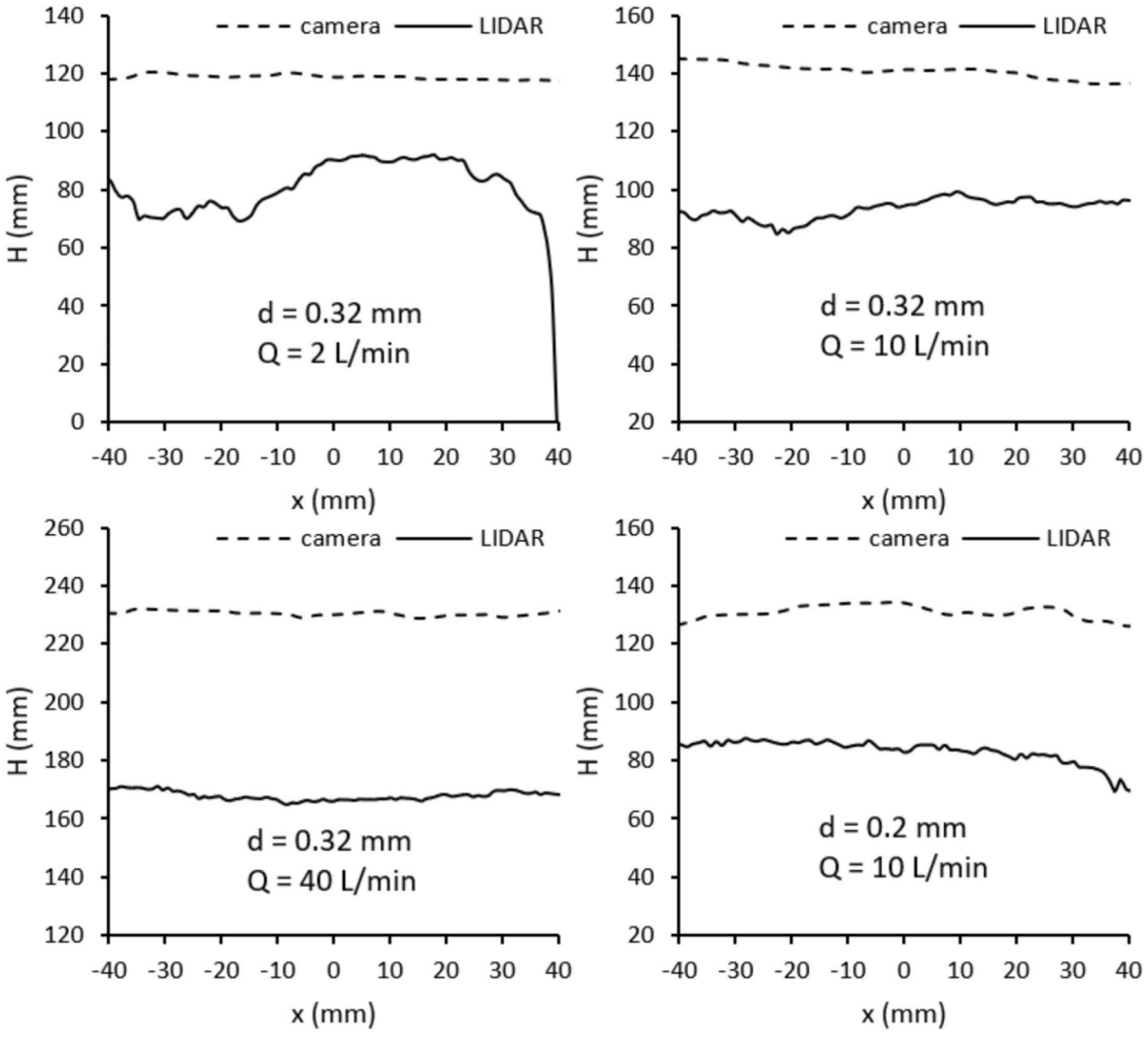

Fig. 6. LIDAR- and camera-measured water height profiles for selected operating conditions.

LIDAR-measured profiles also increases. Also, the fluctuation of $H(x)$ from its mean value is more significant in operating points with low aeration rates, particularly in the case of $Q = 2$ L/min. When a small amount of bubbles occurs throughout the vertical water column, the laser device also receives reflections from submerged bubbles and the average measured distance shows greater values and consequently too low water surface [17]. If the laser scanner measures the distance based on the ToF principle, the slower speed of light in the water further contributes to a longer ToF and consequently a longer measured distance (lower water surface).

The effect of water aeration on the LIDAR method performance can be assessed by comparison to high-speed image processing results. The relative measurement error E will be defined as

$$E = \frac{L - L_R}{L_R} \tag{2}$$

In Eq. (2), L is the median distance from the LIDAR receiver to the water surface measured by laser ranging, while L_R is its camera-measured counterpart serving as a reference value (Fig. 5d). Relative distance measuring errors are shown in Fig. 7 as a function of air flow rate Q and plate perforation arrangement. Along with these results, the standard deviation of water surface level, $\sigma_L(x) = \mathrm{std}(L(x,t))$, is presented in Fig. 8.

As seen from Figs. 7 and 8, the highest measurement error E was 20.8 % for still (unaerated) water surface, also coinciding with the highest standard deviation ($\sigma_L = 40.1$ mm). Slight flow aeration of only 2 L/min caused the error to drop sharply to below 6 % and σ_L to 24.3 mm, while the lowest measurement error of 5.5 % was observed at $Q = 5$ L/min. With a further increase in Q, the error E also gradually increased to approximately 10–12 % and 10–17 % at 40 L/min and 70 L/min, respectively. In absolute terms, the measurement error was in the range of 38–94 mm, which is by 1–2 orders of magnitude higher than for scanning solid surfaces (±1 mm). The plate perforation arrangement also affects the measurement error, with 0.5 mm holes yielding lowest errors under most aeration flow rates. On the other hand, the plate with 0.2 mm perforations produced the largest measurement errors and standard deviations under most aeration flow rates. Large σ_L values in aerated water are indicative of larger amplitudes of water surface oscillations. This indicates that for the same aeration rate Q, the higher number of smaller bubbles (plate with $d = 0.2$ mm and $\delta = 11$ mm) results in a more unstable water surface than a lower number of larger bubbles (plates with $d = 0.32$ mm 0.5 mm), thus making LIDAR measurements less reliable. Interestingly, σ_L exhibits a gradual decreasing trend with Q, suggesting that the waving amplitude subsides as air volume fraction becomes high.

Compared to LIDAR measurements, the standard deviation of the camera-measured water level σ_H was significantly lower than σ_L under most operating conditions (Fig. 9). The mostly sub-unity ratio of σ_H/σ_L further validates the feasibility of high-speed imaging as a reference water level measurement method since it proves that the amplitude of visible fluctuations is lower than the LIDAR-detected fluctuation amplitude (if both methods performed equally well, their standard deviations would also be the same). Only at 50 L/min aeration, the camera measurements produced a larger standard deviation than LIDAR (0.32 mm and 0.5 mm plate). This indicates the possibility of increased measurement uncertainty of the optical water surface measurement that could in turn cause the value of E (Eq. (2)) to increase as Q is raised from 40 L/min to 50 L/min. However, further investigation is required.

Although ranging of aerated surfaces is the primary focus of this study, a word of notation is due for unaerated conditions. In the case of an unaerated water column, the large σ_L value is not caused by liquid structure fluctuations since the water is still, but by an irregular reflection pattern. Upon impacting the still water surface, the laser beam can reflect from the surface, or penetrate the water and reflect from the column bottom (perforated plate). This results in a bimodal distribution of LIDAR-measured distances L and consequently larger errors and standard deviations. This also appears to be the case for the 2 L/min aeration conditions – consider a sharp drop of $H(x)$ as x exceeds 40 mm (Fig. 6, upper left panel) despite a very low degree of camera-detected water surface oscillations. This is likely due to locally insufficient aeration, although remarkably the error E was only 5.8 %.

The dependence of laser ranging error on aeration conditions can also be analyzed in dimensionless terms, namely as a function of the air volume fraction α (Eq. (1)). The dependence of LIDAR measurement error on α is shown in Fig. 10. Apart from the already mentioned high error of over 20 % for unaerated conditions, it can be observed that

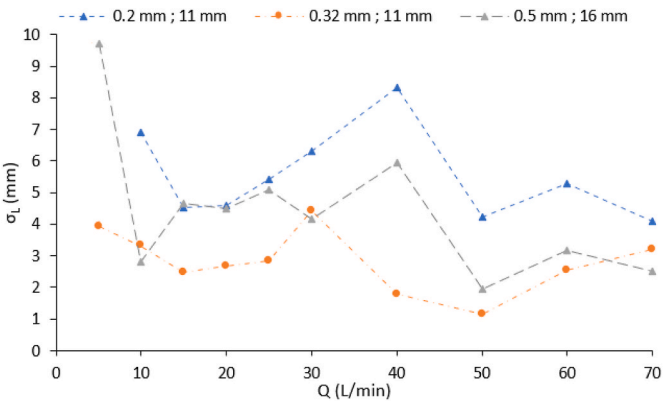

Fig. 8. LIDAR receiver to water surface distance standard deviation at different flow aeration conditions and plate perforation arrangements (still water: $\sigma_L = 40.1$ mm).

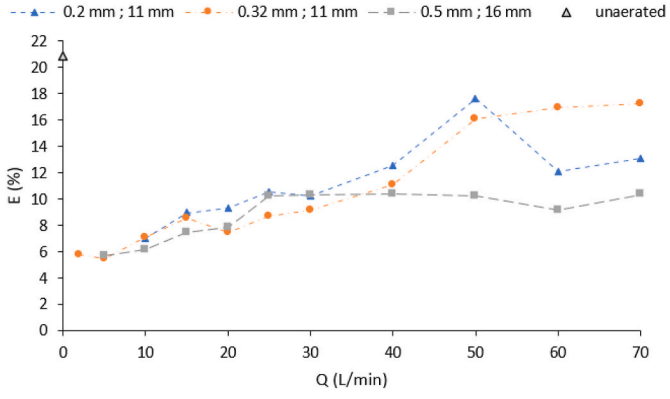

Fig. 7. Relative error of distance measurement from the LIDAR receiver to the water surface at different flow aeration conditions and plate perforation arrangements.

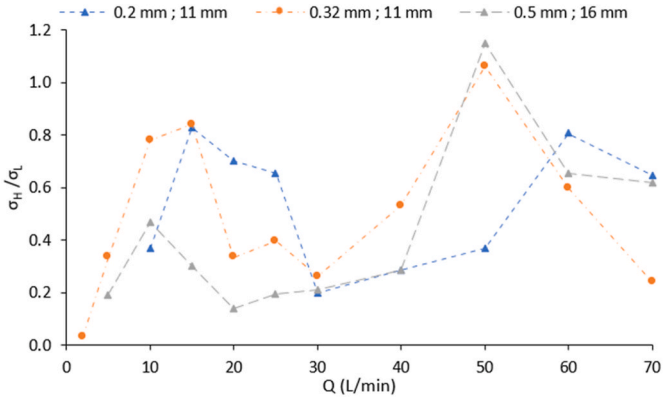

Fig. 9. Ratio of camera-measured to LIDAR-measured water surface distance standard deviation.

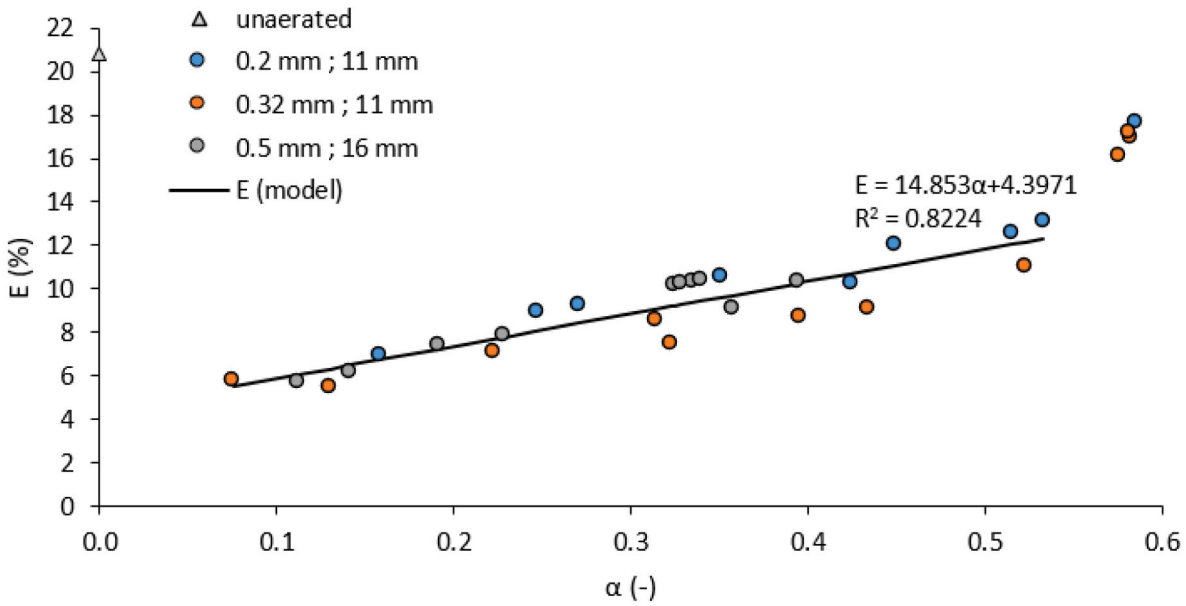

Fig. 10. Dependence of laser ranging relative error on the air volume fraction in the liquid column.

lowest errors occurred around α = 0.1. As α is increased, E increases linearly as seen by the linear model in Fig. 10 following equation $E = 14.85\alpha + 4.40$. The R-squared value was 0.822 when this model was fitted to measured data points with $0.05 < \alpha < 0.55$. Also in this region of α, Fig. 10 suggests an insignificant effect of bubble size on measurement errors. At the highest α values, the error can be seen to rise much more steeply than suggested by the fitted linear trend line. Interestingly, two of these data points with $\alpha > 0.55$ occurred at $Q = 50$ L/min, one at $Q = 60$ L/min and only one at the maximum aeration rate of 70 L/min. This can largely explain why relative errors shown in Fig. 7 do not rise monotonously for 0.2 mm and 0.5 mm perforations.

Based on these findings, it can be concluded that typical scanning LIDAR devices are most accurate under low to moderate aeration conditions with $0.05 < \alpha < 0.2$, while operating with a significantly higher relative error outside of this range. The best ranging efficiency is achieved when bubble size and the number is sufficient that the free water surface is fully covered and the laser beam cannot penetrate deep into the liquid (or even all the way down to the column bottom). If the aeration rate is further increased beyond this point ($Q > 10$ L/min, $\alpha > 0.2$), the increasingly thick foam begins to form on the free surface, resulting in LIDAR beam deflection much above the actual liquid surface.

4. Conclusions

In this paper, the free water surface ranging performance of an AMCW ToF scanning LIDAR device was investigated on a water column with different degrees of aeration (air volume fraction between 0 and 0.6). Reference water level measurements were provided by a high-speed camera. The LIDAR method was shown to perform well in slightly and moderately aerated water, with lowest errors observed around 0.1 air volume fraction where measurement error was about 5 %. Increasing α above this threshold results in a linear increase of measurement error until very high aeration rates (α = 0.55). LIDAR-measured water levels were found to be consistently below camera-measured levels, indicating that reflections occurred below the visible surface (e.g., from submerged bubbles). The deviation between LIDAR and camera-measured surface profiles was especially pronounced in highly aerated flows where intense foaming occurred, with foam evidently penetrated by the laser beam to a depth of several centimeters before eventual reflection. On the other hand, the bubble size appears to have little effect on the measurement error except in cases with over 0.55 air volume fraction where larger bubbles resulted in slightly lower errors. Considering the findings of this study, the best LIDAR measurement accuracy in practical in-field applications can be expected when the free surface is sufficiently aerated to produce consistent laser beam reflections, and when the air entrainment mechanism is unlikely to generate excessive foaming. In the future research, the accuracy of the laser ranging measurement of the free water surface can be further improved by investigating the effects of the laser beam incident angle, wavelength and modulation (amplitude vs. frequency) as well as remission levels that were beyond the scope of the present study.

Author contributions

Conceptualization, B.B., M.H. and G.R.; methodology, B.B., M.H. and G.R.; software, B.B.; validation, B.B., M.H., S.K.R. and G.R.; formal analysis, B.B.; investigation, B.B. and G.R.; data curation, B.B., M.H. and G.R.; writing—original draft preparation, B.B., M.H., S.K.R. and G.R.; writing—review and editing, B.B. and G.R.; visualization, B.B.; supervision, M.H., S.K.R. and G.R.; project administration, M.H., S.K.R.; funding acquisition, M.H., S.K.R. and G.R. All authors have read and agreed to the published version of the manuscript.

Declaration of competing interest

The authors declare that they have no known competing financial interests or personal relationships that could have appeared to influence the work reported in this paper.

Data availability

Data will be made available on request.

Acknowledgements

The authors acknowledge the financial support from the Slovenian Research Agency ARIS research programs P2-0401 “Energy Engineering” and P2-0180 “Water Science and Technology, and Geotechnical Engineering: Tools and Methods for Process Analyses and Simulations, and Development of Technologies” and grant J2-3056 “Development of an optical measuring method for measurement of the turbulent two-

phase flow with free surface".

References

[1] D. Valero, H. Chanson, D.B. Bung, Robust Estimators for Free Surface Turbulence Characterization: a Stepped Spillway application, Flow Meas. Instrum. 76 (2020), https://doi.org/10.1016/j.flowmeasinst.2020.101809. Elsevier Ltd.

[2] F. Zabaleta, F.A. Bombardelli, J.P. Toro, Towards an understanding of the mechanisms leading to air entrainment in the skimming flow over stepped spillways, Environ. Fluid Mech. 20 (2) (2020) 375–392, https://doi.org/10.1007/s10652-019-09729-2. Springer.

[3] G. Rak, M. Hočevar, F. Steinman, Non-intrusive measurements of free-water-surface profiles and fluctuations of turbulent, two-phase flow using 2-D laser scanner, Meas. Sci. Technol. 31 (6) (2020), https://doi.org/10.1088/1361-6501/ab727f. Institute of Physics Publishing.

[4] H. Chanson, X. Leng, H. Wang, Challenging hydraulic structures of the twenty-first century–from bubbles, transient turbulence to fish passage, J. Hydraul. Res. 59 (1) (2021) 21–35, https://doi.org/10.1080/00221686.2020.1871429. Taylor and Francis Ltd.

[5] S. Felder, H. Chanson, Air–water flow patterns of hydraulic jumps on uniform beds macroroughness, J. Hydraul. Eng. 144 (3) (2018), 04017068, https://doi.org/10.1061/(asce)hy.1943-7900.0001402. American Society of Civil Engineers.

[6] H. Chanson, Air Bubble Entrainment in Free-Surface Turbulent Shear Flows, Academic Press, London, 1997.

[7] N.S.L. Rao, B.H. Barczewski, in: N.S.L. Rao, H. Kobus, B.H. Barczewski (Eds.), Characteristics of Self-Aerated Free-Surface Flows, Erich Schmidt Verlag, Berlin, 1975.

[8] I.R. Wood, H. Kobus, H.-P. Koschitzky, P. Volkart, P. Rutschmann, N.L. de S. Pinto, in: I.R. Wood (Ed.), Air Entrainment in Free-Surface Flows, Balkema Publishing, Rotterdam, 1991.

[9] M.v. Muste, in: D.A. Lyn, R. Ettema, V. Nikora, M.H. Garcia, M.v. Muste, D. Admiraal (Eds.), Experimental Hydraulics: Methods, Instrumentation, Data Processing and Management: Volume I: Fundamentals and Methods (IAHR Monographs), Taylor and Francis, New York, 2017.

[10] M.v. Muste, in: J. Aberle, C. Rennie, D. Admiraal, M.v. Muste (Eds.), Experimental Hydraulics: Methods, Instrumentation, Data Processing: Volume II: Instrumentation and Measurement Techniques and Management (IAHR Monographs), CRC Press, Boca Raton, London, New York, Leiden, 2017.

[11] A.T. Troskolanski, in: S. Kolupaila (Ed.), Hydrometry. Theory and Practice of Hydraulic Measurements, Pergamon Press, Oxford, 1960.

[12] C. Gualtieri, H. Chanson, Physical and numerical modelling of air-water flows: an introductory overview, Environ. Model. Software (2021). Elsevier Ltd.

[13] G. Rak, M. Hočevar, S. Kolbl Repinc, L. Novak, B. Bizjan, A review on methods for measurement of free water surface, Sensors 23 (4) (2023) 1842–1859, https://doi.org/10.3390/s23041842.

[14] P. Teng, J. Yang, Modeling and prototype testing of flows over flip-bucket aerators, J. Hydraul. Eng. 144 (12) (2018), 04018069, https://doi.org/10.1061/(ASCE)HY.1943-7900.0001531.

[15] J. Brossard, A. Hemon, E. Rivoalen, Improved analysis of regular gravity waves and coefficient of reflexion using one or two moving probes, Coast Eng. 39 (2–4) (2000) 193–212, https://doi.org/10.1016/S0378-3839(99)00060-5.

[16] G. Zhang, D. Valero, D.B. Bung, H. Chanson, On the estimation of free-surface turbulence using ultrasonic sensors, Flow Meas. Instrum. 60 (2018) 171–184, https://doi.org/10.1016/j.flowmeasinst.2018.02.009. Elsevier Ltd.

[17] G. Rak, M. Hočevar, F. Steinman, Measuring water surface topography using laser scanning, Flow Meas. Instrum. 56 (2017) 35–44, https://doi.org/10.1016/j.flowmeasinst.2017.07.004. Elsevier Ltd.

[18] R. Li, K.D. Splinter, S. Felder, LIDAR scanning as an advanced technology in physical hydraulic modelling: the stilling basin example, Rem. Sens. 13 (18) (2021), https://doi.org/10.3390/rs13183599. MDPI.

[19] L. Montano, S. Felder, LIDAR observations of free-surface time and length scales in hydraulic jumps, J. Hydraul. Eng. 146 (4) (2020), 04020007, https://doi.org/10.1061/(asce)hy.1943-7900.0001706. American Society of Civil Engineers.

[20] C. Mulsow, H.G. Maas, P. Westfeld, M. Schulze, Triangulation methods for height profile measurements on instationary water surfaces, J. Appl. Geodesy 2 (1) (2008) 21–29, https://doi.org/10.1515/JAG.2008.003.

[21] D.B. Bung, Non-intrusive detection of air-water surface roughness in self-aerated chute flows, J. Hydraul. Res. 51 (3) (2013) 322–329, https://doi.org/10.1080/00221686.2013.777373.

[22] J.D. Nóbrega, H.E. Schulz, D.Z. Zhu, Free surface detection in hydraulic jumps through image analysis and ultrasonic sensor measurements, in: ISHS 2014 - Hydraulic Structures and Society - Engineering Challenges and Extremes: Proceedings of the 5th IAHR International Symposium on Hydraulic Structures, University of Queensland, 2014.

[23] D.B. Bung, B.M. Crookston, D. Valero, Turbulent free-surface monitoring with an RGB-D sensor: the hydraulic jump case, J. Hydraul. Res. 59 (5) (2021) 779–790, https://doi.org/10.1080/00221686.2020.1844810. Taylor and Francis Ltd.

[24] M. Palace, F.B. Sullivan, M. Ducey, C. Herrick, Estimating tropical forest structure using a terrestrial lidar, PLoS One 11 (4) (2016), e0154115, https://doi.org/10.1371/journal.pone.0154115. Public Library of Science (PLoS).

[25] G. Spreitzer, J. Tunnicliffe, H. Friedrich, Using Structure from Motion photogrammetry to assess large wood (LW) accumulations in the field, Geomorphology 346 (2019), https://doi.org/10.1016/j.geomorph.2019.106851. Elsevier B.V.

[26] R. Li, K.D. Splinter, S. Felder, Aligning free surface properties in time-varying hydraulic jumps, Exp Therm Fluid Sci 126 (2021), https://doi.org/10.1016/j.expthermflusci.2021.110392. Elsevier Inc.

[27] K. Wang, R. Tang, R. Bai, H. Wang, Evaluating phase-detection-based approaches for interfacial velocity and turbulence intensity estimation in a highly-aerated hydraulic jump, Flow Meas. Instrum. 81 (2021), https://doi.org/10.1016/j.flowmeasinst.2021.102045. Elsevier Ltd.

[28] K. Martins, C.E. Blenkinsopp, H.E. Power, B. Bruder, J.A. Puleo, E.W.J. Bergsma, High-resolution monitoring of wave transformation in the surf zone using a LiDAR scanner array, Coast. Eng. 128 (2017) 37–43, https://doi.org/10.1016/j.coastaleng.2017.07.007. Elsevier B.V.

[29] B. Behroozpour, P.A.M. Sandborn, M.C. Wu, B.E. Boser, Lidar system architectures and circuits, IEEE Commun. Mag. 55 (10) (2017) 135–142, https://doi.org/10.1109/MCOM.2017.1700030. Institute of Electrical and Electronics Engineers Inc.

[30] M. Kramer, H. Chanson, Optical flow estimations in aerated spillway flows: filtering and discussion on sampling parameters, Exp Therm Fluid Sci 103 (2019) 318–328, https://doi.org/10.1016/j.expthermflusci.2018.12.002. Elsevier Inc.

[31] H. Chanson, Hydraulics of aerated flows: qui pro quo, J. Hydraul. Res. 51 (3) (2013) 223–243, https://doi.org/10.1080/00221686.2013.795917.

[32] S. Felder, L. Montano, H. Cui, W. Peirson, M. Kramer, Effect of inflow conditions on the free-surface properties of hydraulic jumps, J. Hydraul. Res. 59 (6) (2021) 1004–1017, https://doi.org/10.1080/00221686.2020.1866692. Taylor and Francis Ltd.

[33] F. Jiang, W. Xu, J. Deng, W. Wei, Flow structures of the air-water layer in the free surface region of high-speed open channel flows, Math Probl Eng 2020 (2020), https://doi.org/10.1155/2020/5903763. Hindawi Limited.

[34] H. Chanson, S. Aoki, A. Hoque, Bubble entrainment and dispersion in plunging jet flows: freshwater vs. Seawater, J. Coast Res. 22 (3) (2006).

[35] SICK 2D LiDAR sensors. https://cdn.sick.com/media/docs/0/90/790/operating_instructions_lms4000_2d_lidar_sensors_en_im0079790.pdf, 2022.